1986

A Mathematical Model of a Zn/Br2 Cell on Charge

M J. Mader
Texas A & M University - College Station

Ralph E. White
University of South Carolina - Columbia, white@cec.sc.edu

Publication Info

Journal of the Electrochemical Society, 1986, pages 1297-1307.

Publisher's Version: http://dx.doi.org/10.1149/1.2108857
DOI: 10.1149/1.2108857

A Mathematical Model of a Zn/Br_2 Cell on Charge

M. J. Mader and R. E. White*

Department of Chemical Engineering, Texas A&M University, College Station, Texas 77843

ABSTRACT

A mathematical model of a parallel plate electrochemical cell with a separator and a homogeneous bulk reaction is presented. The model is based on the Zn/Br_2 redox couple and can be used as an aid for the design of an efficient rechargeable storage battery. It is shown that four independent variables exist for the system at a fixed temperature: the effective separator thickness, the residence time, the channel width, and the potential driving force. Performance criteria of interest for the Zn/Br_2 battery are defined. Predictions of performance during the charging process are presented. It is shown that the cell performance improves as the effective thickness of the separator is increased, despite the associated greater cell resistance. It is also shown that a change in the residence time has little effect on cell performance.

Several companies, including Exxon and Energy Research Corporation (ERC), are pursuing the development of a zinc/bromine (Zn/Br_2) battery by building and testing various designs (1). A comprehensive mathematical model which can reasonably predict the performance of a Zn/Br_2 battery could be of great use to these companies as a tool for designing a more efficient system. Such a model would reduce the need to build and test dozens of designs.

A typical Zn/Br_2 flow battery consists of stacks of electrochemical cells in which reversible reactions occur at the electrodes. An aqueous electrolyte solution containing the reacting species is circulated through each cell in a stack and stored in external tanks. To charge the battery, a current or potential is applied to the stack while the fluid is fed to each cell from the external tanks. Energy is stored in the form of Zn and Br_2 when zinc ions (Zn^{2+}) in solution are plated as solid Zn on the cathode and bromide ions (Br^-) react within a porous layer on the anodes to form Br_2, a liquid which is soluble in the aqueous solution. However, any Br_2 that reaches the Zn electrode reacts electrochemically, thereby causing a loss of charge. To help prevent this undesirable reaction, either a separator or a complexing salt which causes an inert, insoluble Br_2-rich phase to be formed, or both, are included. An additional reaction which occurs, in the bulk of the electrolytic solution, is the partial complexation of Br_2 and Br^- to tri-bromide ions (Br_3^-). The battery is discharged by circulating the stored electrolyte through the cell stack with the terminal leads of the cell stack connected to an appropriate load. The reverse of the electrochemical reactions occur at each electrode and energy is released.

In the work presented here, an attempt has been made to include as many of these features as possible into a comprehensive two-dimensional Zn/Br_2 cell model. The goal is to create a cell model from which a greater understanding of the physical phenomena affecting cell performance can be obtained and which gives reasonable performance predictions. The model presented, therefore, is derived to the greatest extent possible from scientific first principles, with a de-emphasis on empirical relationships such as mass transfer coefficients. The scope of this work does not allow all the features of a typical Zn/Br_2 cell design to be included. Only a charge mode for a single cell in the stack is considered. The electrochemical energy storage reactions producing Br_2 and Zn are included, but the Br_2 electrode is modeled without a porous layer. The undesirable Br_2 reaction competing with the Zn reaction at the cathode is included in the model. A porous separator placed between the two electrodes is in the model, but the second, Br_2-rich phase has not been considered. Finally, the complexation of Br_2 and Br^- to Br_3^- has been included in the model. In addition, a one-dimensional model, called a one-step model, which requires significantly less computation time, yet compares very well to the two-dimensional solution, has been developed.

*Electrochemical Society Active Member.

Analysis of the model provides a set of independently adjustable parameters which are shown to control the performance of the system. To study the effect of physical phenomena on cell performance, performance criteria are defined and the independently adjustable parameters are varied. Results of the variations lead to an understanding of the complex interaction of kinetic, thermodynamic, and transport properties within the cell.

The Zn/Br_2 cell model presented is the first model developed which predicts product conversion, energy efficiency, and other quantities of practical interest to a cell designer, for a separated cell in which multiple electrode reactions occur. White *et al.* (2) developed a mathematical model of a parallel plate electrochemical reactor (PPER) which can predict similar quantities of interest but does not include a separator. Their work is the most desirable from which to develop a Zn/Br_2 cell model, because they start from first principles and include many of the same features present in a typical Zn/Br_2 cell. Lee and Selman (3, 4) developed a comprehensive model of a Zn/Br_2 cell but their work does not address at all the objectives desired in this work. Van Zee *et al.* (5) developed a Zn/Br_2 battery model which determines an energy efficiency for the entire battery but cannot predict product conversions. Fedkiw and Watts (6) developed a comprehensive model of the iron/chromium (Fe/Cr) redox battery, which, unfortunately, cannot be used for the Zn/Br_2 battery presented here.

White *et al.* (2) developed a mathematical model of an electrochemical reactor which, with a few modifications, is useful in developing a model of a Zn/Br_2 cell. The model of White *et al.* (2) consists of parallel plate electrodes and an electrolyte in laminar flow between them. Their model uses a differential mass balance in two dimensions and can handle multiple electrode reactions, as well as homogeneous reactions in the electrolyte bulk. Additionally, their model can be used to predict current efficiencies and conversions per pass of each species in solution. The model of White *et al.* (2) is extended here to treat the Zn/Br_2 battery.

Lee and Selman (3, 4) modeled the Zn/Br_2 system with a separator, with the particular interest of studying dendrite growth due to uneven plating of Zn. They consider the Zn/Br_2 cell as a complete unit. However, their model does not address the goals described above for the following reasons. First of all, they consider cell performance only at fixed, typical states of charge and do not vary design parameters, such as electrode length or separator thickness. Second, Lee and Selman propose corrosion of Zn as a possible reaction during charge, while it is felt here that corrosion could not occur on charge due to cathodic protection. Finally, Lee and Selman characterize their separator with parameters such as porosity and a mass-transfer coefficient which are difficult to determine experimentally. Van Zee (7) has shown that the MacMullin number, N_m, is an easily determined characteristic of a porous separator which, with the separator thickness, can completely describe its transport properties.

Van Zee *et al.* (5) developed a simple Zn/Br_2 battery model in which they estimate cell resistances and total energy requirements to run the battery. They have found that by varying the separator thickness the energy efficiency may be increased by at least 1%, which is a considerable energy savings for an often-cycled battery. Their model is limited, however, because it does not include the capability of predicting product conversion. Also, their model does not include the effect of fluid flow rate on cell performance, such as how the flow rate affects the coulombic losses caused by the reduction of bromine at the zinc electrode on charge.

Fedkiw and Watts (6) have simulated an electrochemical cell which includes a separator and multiple electrode reactions, but they focus on the Fe/Cr redox system which uses porous packed bed electrodes. Their model includes studies at various states of charge, and they follow concentration changes as well as local current densities. Because they study the Fe/Cr system and have done only a small amount of work varying design parameters, their work is not helpful in understanding the Zn/Br_2 system. Also, they have preferred to study power requirements and current flow rather than concentration changes, which are of interest in this work.

Model Development

The assumptions needed to develop the model are presented first, followed by the governing equations and boundary conditions.

Assumptions.—A schematic of a single cell for the Zn/Br_2 battery is pictured in Fig. 1. It features a parallel plate reactor with a porous separator. Electrolyte is pumped to each side of the cell from separate tanks. The aqueous electrolytic solution consisting of the species Na^+, Br^-, Br_2, Br_3^-, and Zn^{2+} flows laminarly in the channels on both sides of the separator. It is assumed that species diffuse and migrate through the separator. However, to simplify the analysis, it is assumed that the pressure drop per unit length is identical on both sides of the cell, thereby preventing convective flow through the separator. This assumption is achieved by setting $S_A = S_C$ and $v_{avg} = v_{avg,A} = v_{avg,C}$.

The length (L) and width (W) of both electrodes are assumed to be large relative to the gap between the electrodes (S). Nguyen *et al.* (8), in an extension of the model of White *et al.* (2), determined that if the aspect ratio ($\alpha = S/L$) is less than 0.2, then the axial diffusion and migration flux terms may be neglected. It is assumed that the mobility of ionic species follows the Nernst-Einstein equation ($u_i = D_i/RT$) and that the Butler-Volmer equation can be used to describe the electrochemical reactions. In addition, pseudo-steady-state conditions are assumed to exist. That is, it is assumed that because of a low conversion per pass, the concentration of the feed to the cells, within the external storage tanks, changes very slowly.

On charge, the reactions that are assumed to take place at the electrodes are

$$Br^- \rightarrow 1/2\ Br_2 + e^- \qquad \text{(anode, reaction 1)}$$

$$1/2\ Br_2 + e^- \rightarrow Br^- \qquad \text{(cathode, reaction 2)}$$

$$1/2\ Zn^{2+} + e^- \rightarrow 1/2\ Zn \qquad \text{(cathode, reaction 3)}$$

Reaction 1 and 3 are the desired reactions which lead to energy storage. Reaction 2 is an undesired self-discharge reaction which leads to inefficiency and energy losses. Corrosion of Zn by Br_2 during charge according to

$$Zn + Br_2 \rightarrow ZnBr_2$$

has been proposed by Lee and Selman (3, 4), but during charge, the zinc is cathodically protected, and thus corrosion is at least negligible and probably nonexistent. Due to the large voltaic driving force, hydrogen evolution at the cathode might be proposed, but this reaction has a small exchange current density on zinc electrodes. In addition, the solution is assumed to have a large enough pH that there is no appreciable concentration of hydrogen ion.

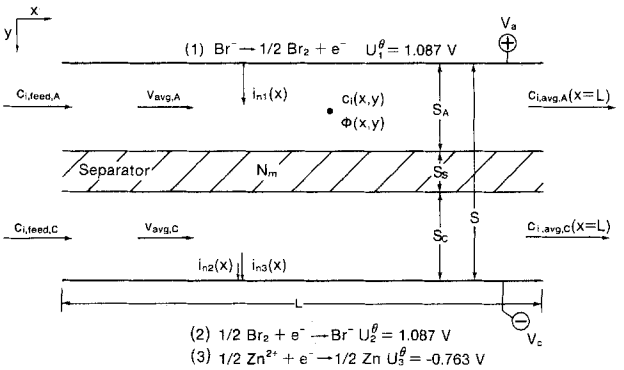

Fig. 1. Schematic of an individual cell in a Zn/Br_2 battery

A homogeneous complexation reaction producing Br_3^-

$$Br_2 + Br^- \rightleftharpoons Br_3^- \qquad \text{(bulk, reaction 4)}$$

occurs in the solution bulk. It is assumed this reaction is fast and, thus, the concentrations of the three species are in equilibrium throughout the cell, according to the equilibrium constant given by Eigen and Kustin (9)

$$K_{eq} = \frac{c_{Br_3^-}}{c_{Br^-}\ c_{Br_2}} = 17M^{-1} = 17{,}000\ (\text{mol/cm}^3)^{-1} \qquad [1]$$

Governing equations.—The cell in Fig. 1 is divided into three sections, two electrolyte flow channels of width S_A, and a separator of width S_S. The governing equations for each section, as developed in the PPER model of White *et al.* (2), include the electroneutrality condition and a steady-state material balance equation for each species. The equations may be used to solve for the concentration (c_i) and potential (Φ) distributions as functions of the axial (x) and radial (y) position.

The electroneutrality condition

$$\sum_i z_i c_i = 0 \qquad [2]$$

ensures that there is no buildup of positive or negative charge anywhere in the electrolytic solution. For steady state, the material balance equations for each species are

$$-\nabla \cdot \mathbf{N}_i + R_i = 0 \qquad (i = Br^-, Br_2, Br_3^-) \qquad [3]$$

$$\nabla \cdot \mathbf{N}_i = 0 \qquad (i = Na^+, Zn^{2+}) \qquad [4]$$

where

$$\mathbf{N}_i = -D_i \nabla c_i - z_i \frac{D_i}{RT} \mathbf{F} c_i \nabla \Phi + \mathbf{v} c_i \qquad \text{(flow channels)} \qquad [5]$$

and

$$\mathbf{N}_i = -D_{i,e} \nabla c_i - z_i \frac{D_{i,e}}{RT} \mathbf{F} c_i \nabla \Phi \qquad \text{(separator)} \qquad [6]$$

In the separator, an effective diffusivity, $D_{i,e}$, is required, given by Van Zee (7) as

$$D_{i,e} = \frac{D_i}{N_m} \qquad [7]$$

where N_m is the MacMullin number. The MacMullin number is a characteristic of a porous separator, equivalent to the ratio of the separator's tortuosity to its porosity. However, unlike porosity or tortuosity, it is easily determined and not a property of solution strength, as shown by Van Zee (7). The MacMullin number is given by a resistivity ratio

$$N_m = \frac{\rho}{\rho_o} \qquad [8]$$

where ρ_o is the resistivity of a solution without a separa-

tor in its midst, and ρ is the resistivity of separator and solution together.

The velocity distribution within the flow channels is assumed to be well-developed laminar flow as given by (10)

$$v_y = 0; \quad v_x = 6v_{avg}\left(\frac{y}{S_A} - \frac{y^2}{S_A{}^2}\right) \qquad [9]$$

The material balance equations given by Eq. [3] can be simplified by assuming that reaction [4] is at equilibrium so that $R_{Br^-} = R_{Br_2} = -R_{Br_3^-}$. For the species Br^- and Br_3^-, Eq. [3] for each can be added to get

$$(-\nabla \cdot \mathbf{N}_{Br^-} + R_{Br^-}) + (-\nabla \cdot \mathbf{N}_{Br_3^-} + R_{Br_3^-}) = 0 \qquad [10]$$

which reduces to a governing equation consisting only of flux terms

$$\nabla \cdot \mathbf{N}_{Br^-} + \nabla \cdot \mathbf{N}_{Br_3^-} = 0 \qquad [11]$$

Likewise for species Br_2 and Br_3^-

$$\nabla \cdot \mathbf{N}_{Br_2} + \nabla \cdot \mathbf{N}_{Br_3^-} = 0 \qquad [12]$$

Since the number of equations has been reduced by one, the equilibrium expression of Eq. [1] is needed to describe the system fully. Therefore, Eq. [1], [2], [4], [11], and [12] comprise the set of governing equations needed to solve the system for the unknown variables, c_i and Φ.

As postulated by White *et al.* (2) and later demonstrated by Nguyen *et al.* (8), when the aspect ratio ($\alpha = S/L$) is small, then the diffusion and migration terms of the flux expression in the axial, or flow, direction are negligible compared to the radial or normal diffusion and migration terms. Thus, upon converting to the dimensionless variables

$$\zeta = x/L \qquad [13]$$

$$\eta = y/S \qquad [14]$$

$$\eta' = \begin{cases} \dfrac{y}{S_A} & 0 < y < S_A \\ \dfrac{y - (S_A + S_S)}{S_C} & (S_A + S_S) < y < S \end{cases} \qquad [15]$$

$$\theta_i = c_i/c_{i,ref} \qquad [16]$$

$$Pe = \frac{2Sv_{avg}}{D_R} \qquad [17]$$

the divergence of the flux of species i in Eq. [4], [11], and [12] may be rewritten for the flow channels as

$$\frac{S^2}{c_{i,ref}D_i}(\nabla \cdot \mathbf{N}_i) = -\frac{\partial^2\theta_i}{\partial\eta^2} - \frac{z_i\mathbf{F}}{RT}\left[\theta_i\frac{\partial^2\Phi}{\partial\eta^2} + \frac{\partial\theta_i}{\partial\eta}\frac{\partial\Phi}{\partial\eta}\right] + 3\frac{D_R}{D_i}Pe\alpha(\eta' - \eta'^2)\frac{\partial\theta_i}{\partial\zeta} \qquad [18]$$

and for the separator as

$$\frac{S^2}{c_{i,ref}D_{i,e}}(\nabla \cdot \mathbf{N}_i) = -\frac{\partial^2\theta_i}{\partial\eta^2} - \frac{z_i\mathbf{F}}{RT}\left[\theta_i\frac{\partial^2\Phi}{\partial\eta^2} + \frac{\partial\theta_i}{\partial\eta}\frac{\partial\Phi}{\partial\eta}\right] \qquad [19]$$

Note that two dimensionless radial variables are used in Eq. [18]. The variable η is made dimensionless by the total electrode gap S, and is used to define the step size in any section when converting the differential governing equations to finite difference form. The variable η' is made dimensionless by the flow channel width S_A, and is needed to express position within the flow channels, since the local electrolyte velocity depends on the relative position within the channel. Note also that the Peclet number is defined here in terms of S (Eq. [17]) instead of S_A, which would be more appealing physically; however, since no dimensionless analysis is presented in this paper, the definition of Pe is arbitrary.

Initial and boundary conditions.—To complete the system of equations, the initial and boundary conditions must be specified. Conditions are specified at the cell entrance, the electrodes, and the electrolyte/separator interface.

The initial conditions at the cell entrance and boundary conditions at the electrodes are the same as specified by White *et al.* (2). At the cell entrance, the feed concentrations are known, and the electroneutrality condition must hold

$$\text{at } \zeta = 0 \qquad \theta_i = \theta_{i,feed}; \qquad \sum_i z_i c_{i,ref}\theta_{i,feed} = 0 \qquad [20]$$

The boundary conditions at the electrodes are that the electroneutrality condition holds and that the rate of consumption or production of a species by electrochemical reaction at the electrode is equal to the net normal flux of the species toward or away from the electrode. That is

$$\text{at } \eta = 0 \quad \text{(anode)} \quad \frac{s_{ij}i_{nj}}{n_j\mathbf{F}} = -N_{ni} \qquad [21]$$

and

$$\text{at } \eta = 1 \quad \text{(cathode)} \quad \frac{s_{i2}i_{n2}}{n_2\mathbf{F}} = N_{ni}, \quad \frac{s_{i3}i_{n3}}{n_3\mathbf{F}} = N_{ni} \qquad [22]$$

where i_{nj} is the current density for reaction j, s_{ij} is the stoichiometric coefficient for each species in the electrochemical reaction, n_j is the number of electrons transferred in the reaction, and N_{ni} is the net normal flux of species i, in which the derivatives are defined to be in the positive y direction. It should be pointed out that the signs used for N_{ni} in Eq. [21] and [22] are consistent with the convention that positive current leaves the anode to enter the electrolytic solution, and negative current from the solution enters the cathode.

The normal component of the current density for reaction j, i_{nj}, is given by the Butler-Volmer equation, as given by White *et al.* (11)

$$i_{nj} = i_{oj,ref}\left\{\prod_i (\theta_{i,o})^{p_{ij}}\exp\left(\frac{\alpha_{aj}\mathbf{F}}{RT}\eta_j\right) - \prod_i (\theta_{i,o})^{q_{ij}}\exp\left(\frac{-\alpha_{cj}\mathbf{F}}{RT}\eta_j\right)\right\} \qquad [23]$$

where $\theta_{i,o}$ is a dimensionless local surface concentration and η_j is the reaction overpotential, defined as

$$\eta_j = V_e - \Phi_{oe} - U_{j,ref} \qquad [24]$$

In Eq. [24], V_e is the electrode potential (either V_a or V_c), Φ_{oe} is the potential of the solution at the surface of that electrode (either Φ_{oa} or Φ_{oc}), and $U_{j,ref}$ is the local open-circuit potential of reaction j at the reference concentrations. The open-circuit potential is a thermodynamic parameter of the solution given by

$$U_{j,ref} = U_j{}^\theta - U_{RE}{}^\theta - \frac{RT}{n_j\mathbf{F}}\sum_i^n s_{ij}\ln\left(\frac{c_{i,ref}}{d_o}\right) + \frac{RT}{n_{RE}\mathbf{F}}\sum_i^n s_{i,RE}\ln\left(\frac{c_{i,RE}}{d_o}\right) \qquad [25]$$

with the subscript RE referring to an arbitrary reference electrode. V_e, Φ_{oe}, $U_j{}^\theta$, and $U_{RE}{}^\theta$ are all defined relative to a reference electrode.

The boundary conditions at the separator/electrolyte interface are that the electroneutrality condition holds (as it

does everywhere in the reactor) and that the normal flux of each species is continuous across the interface. That is, at the anolyte/separator interface

$$\text{at } y = S_A \qquad N_{ni,A} = N_{ni,S} \qquad [26]$$

Expanding with the normal flux terms in Eq. [5] and [6] and converting to dimensionless quantities, this boundary condition becomes

$$\text{at } y = S_A \quad -\left(\frac{\partial\theta_i}{\partial\eta}\right)_A - \frac{z_i\mathbf{F}}{RT}\theta_i\left(\frac{\partial\Phi}{\partial\eta}\right)_A = -\frac{1}{N_m}\left(\frac{\partial\theta_i}{\partial\eta}\right)_S - \frac{z_i\mathbf{F}}{RT}\theta_i\frac{1}{N_m}\left(\frac{\partial\Phi}{\partial\eta}\right)_S \qquad [27]$$

where $\partial\theta_i/\mathrm{B}\eta$ and $\partial\Phi/\mathrm{B}\eta$ are evaluated at the interface, but wholly within the region of their respective subscript. Note that D_i has been canceled from this equation, but the MacMullin number, N_m, does not cancel. At the separator/catholyte interface, the boundary condition is similar.

In an effort to cut down on calculation time, a simple model was developed in which only one step was taken in the flow direction [see Mader *et al.* (12)]. This model assumes that i_{nj} is a constant along the length of the reactor and therefore not a function of ζ as in the previous case. Similarly, c_i and Φ become functions of η only. In this way, the cell acts much like a CSTR in the flow direction. At a given value of η, there is only a step change in concentration of a species from its feed value to its exit value, instead of a gradual concentration gradient down the length of the reactor as in the more complicated model. (To distinguish the two models, the simple one will be called the one-step model and the other the continuous model.)

In the one-step model, a finite difference expression over the length of the reactor replaces the axial concentration gradient in the convection term of the continuous model

$$\frac{\partial c_i}{\partial x} \approx \frac{c_i - c_{i,feed}}{L} \qquad [28]$$

In dimensionless coordinates, with $c_{i,ref} = c_{i,feed}$, Eq. [28] becomes

$$\frac{\partial\theta_i}{\partial\zeta} \approx \frac{\theta_i - 1}{1} \qquad [29]$$

All other equations from the continuous model remain the same in the one-step model.

Because it essentially becomes a one-dimensional model, the one-step model is a less accurate solution of the electrochemical cell than the two-dimensional continuous model. However, the one-step model does retain the concepts of radial gradients across the cell and the possibility of multiple electrode reactions occurring at each electrode. In addition, the one-step model requires less computer time to solve. The accuracy of the one-step model relative to the continuous model essentially depends on the conversion per pass of the system. The assumption that the concentration in the flow direction is uniform is reasonable for a system only if the conversion per pass is small, as is often the case for a Zn/Br_2 cell.

Parameters.—The parameters used in the model consist of the fixed parameters of the cell and the independently adjustable parameters. The fixed parameter values used in the Zn/Br_2 cell model are given in Table I. The system was set up to simulate as closely as possible the design of Exxon (5, 13, 14) from which the most design parameters were available. The feed composition at initial conditions, $\theta_{i,feed}$, is assumed to be the same in both channels, for convenience. To determine the concentration of each species in the feed, it is first assumed that the solution is composed of Na^+, Br^-, Br_2, and Zn^{2+} at the reference concentrations listed in Table I, and that Br^- and Br_2 are uncomplexed. Then, an equilibrium calculation is done using the tri-bromide complexation reaction and K_{eq} to determine the adjusted concentrations of Br^- and Br_2, and the corresponding equilibrium concentration of Br_3^-. After all other parameters were set, the exchange current densities $i_{oj,ref}$ were picked by trial and error to give current densities similar to that reported by Exxon (13). When compared to values in the literature (19, 20), these $i_{oj,ref}$ were within an order of magnitude.

Table I. Fixed parameter values for the Zn/Br_2 cell

Kinetic and thermodynamic (T = 298.15 K, V_c = 0.0V)

Reaction (j)	$i_{oj,ref}$[a] (A/cm²)	α_{aj}	α_{cj}	n_j	U_j^{θ}[b] (V)	$U_{j,ref}$[c] (V)
1	0.0031	0.5	0.5	1	1.087	1.783
2	0.0031	0.5	0.5	1	1.087	1.783
3	1.00	0.5	0.5	1	−0.763	0.0

Reaction 4 (Homogeneous, bulk) K_{eq}[d] = 17000 (mol/cm³)⁻¹

Stoichiometry and electrochemical reaction orders

Species (i)	Reactions [1] and [2] (j = 1, 2) s_{ij}	p_{ij}	q_{ij}	Reaction [3] (j = 3) s_{ij}	p_{ij}	q_{ij}
Na^+	0	0	0	0	0	0
Br^-[e]	1	1	0	0	0	0
Br_2	−1/2	0	1/2	0	0	0
Zn^{2+}[f]	0	0	0	−1/2	0	1/2
Br_3^-	0	0	0	0	0	0

Transport and reference concentrations

Species (i)	z_i	D_i[g] (cm²/s) × 10^5	$c_{i,ref}$ (mol/cm³) × 10^3	$\theta_{i,feed}$[h]
Na^+	1	1.334	1.00	1.000
Br^-	−1	2.084	3.00	0.983
Br_2	0	1.310	0.05	0.0203
Zn^{2+}	2	0.754	1.00	1.000
Br_3^-	−1	1.310	0.10	0.510

[a] Chosen to duplicate current densities reported in Ref. (13).
[b] See Ref. (15).
[c] The reference electrode is reaction [3] at the reference conditions.
[d] See Ref. (9).
[e] Limiting reactant at Br_2 electrode.
[f] Limiting reactant at Zn electrode.
[g] See Ref. (16-18); $D_{Br_3^-}$ assumed equal to D_{Br_2}.
[h] At initial charging conditions, the feed to each channel is assumed to be the same, for convenience.

The model input variable parameters are the length of the electrode (L), the average velocity of the electrolyte (v_{avg}), the flow channel width (S_A), the thickness of the separator (S_S), the MacMullin number (N_m), and the applied cell potential ($E_{cell} = V_a - V_c$). Note that the total electrode gap (S) is a linear combination of the flow channel widths and the separator thickness, and is therefore not an input variable, since it is completely specified by the other widths. Upon reviewing the governing equations and boundary conditions and analyzing the model results, it is found that only four independently adjustable parameters exist in the model, although six input variables may be specified. A meaningful set of independent parameters consists of the residence time of the electrolyte in the cell, L/v_{avg} (which appears as a ratio in the term Peα), the flow channel width, S_A (which appears alone as the denominator in the definition of η'), the effective separator thickness, N_mS_S (which appears as a product in the denominator of the finite difference form of Eq. [27], as shown in Ref. (21)), and the cell potential, E_{cell} (since V_a and V_c are relative to the same reference potential). Van Zee (7) showed in a separator flow-through experiment that the product N_mS_S is important as a group, and not N_m or S_S separately. In the case of the Zn/Br_2 cell, the model indicates that N_mS_S is also an independent variable for flow by a separator.

In this study, each of the individual parameters, L, v_{avg}, S_A, S_S, N_m, and E_{cell} are set at values to be expected in a typical Zn/Br_2 battery. The parameter L/v_{avg} is varied by changing either L or v_{avg}, or both, between runs. The length, L, is varied between 20 and 30 cm in this study, while v_{avg} is varied between 2.0 and 1.5 cm/s. The channel flow width (S_A) is assigned values between 0.005 and 0.10 cm. Either N_m or S_S is varied to alter N_mS_S, with N_m varying between 1.5 and 10.0, and S_S between 0.02 and 0.12 cm. For E_{cell}, V_c is set equal to 0 V for convenience, and V_a is varied between 1.85 and 2.025V.

Solution Technique and Material Balance Closure

Having set the fixed and variable parameters, the system equations can be solved for the concentration and potential distributions by using an implicit stepping technique in the axial direction (for the two-dimensional model) and Newman's technique (16) in the radial direction. This solution procedure is discussed by White *et al.* (2) and Mader *et al.* (12). To ensure that the average current densities predicted by the model are consistent with the predicted average exit concentrations of each species, a material balance closure is done on each species. At steady state, the molar (or mass) rate of consumption or production of a species by electrochemical and homogeneous reaction within the cell must equal the net molar (or mass) flow rate of that species through the reactor from entrance to exit. A quantitative evaluation of the material balance closure statement was done for each case studied and the model predictions were found to be consistent each time. Further information on this test for consistency can be found by referring to Mader (21).

Results and Discussion

Once the consistency of the solution technique is verified, the concentration and potential distributions can be used to analyze the Zn/Br_2 cell model. First, performance criteria of specific interest to this cell are derived. Then, N_mS_S is verified as an independent parameter. Next, the two-dimensional model and one-step model predictions are compared. Examples of performance predictions that can be obtained from the Zn/Br_2 cell model at initial charging conditions are then presented. Finally, the performance of the cell as a function of the state of charge of the system is considered for three values of the effective separator thickness, N_mS_S, and three values of the residence time.

Performance criteria.—To develop a meaningful set of performance criteria for the Zn/Br_2 cell, the desirable characteristics of a rechargeable battery system should be considered. First, it is important to keep the cell current at a relatively low level to prevent dendritic growth of zinc during charging. Second, it is important that a rechargeable battery can be charged quickly. A third desirable characteristic, during the charging process, is a low amount of energy consumption relative to the amount of product stored. Finally, it is important to have a high energy efficiency, indicating the energy consumed has been put to useful work.

To monitor the cell current, the average current density at an electrode, i_{avg}, is a useful quantity. It is defined as the sum of the average current densities for each reaction at an electrode

$$i_{avg} = \left| \sum_j i_{nj,avg} \right| \qquad [30]$$

where $i_{nj,avg}$ is an average of the local current densities, $i_{nj}(x)$, over the length of the electrode. The value of $i_{nj,avg}$ is solved for directly in the one-step model.

The average current density may also be defined as the total cell current, I, per surface area of electrode, LW, so that for electrodes of equal surface area, the value of i_{avg} must be the same at both electrodes.

A second desirable characteristic is the capability to charge quickly. In other words, for a given area of electrode, it is important to achieve a high production rate of the species which must be stored to charge the battery. For the Zn/Br_2 cell to charge, Br_2 must be produced at the anode and stored in the anolyte and Zn must be plated at the cathode. Since the electrode material is often one of the largest costs in the battery, it is important to characterize the production rate in terms of the surface area of electrode required.

Bromine is stored in the anolyte in two forms, either as dissolved liquid Br_2 or as part of the ionic complex Br_3^-. Br_2 is produced at the anode during charge by reaction of Br^-. Most of the Br_2 produced at the anode is complexed with excess Br^- to create Br_3^-. Some of the bromine, both as liquid Br_2 and as the complexed Br_3^-, may diffuse out of the anolyte into the separator, while some may enter the anolyte from the separator, depending on the concentration and potential gradients. However, only the bromine which exits the reactor in the anolyte, as either Br_2 or Br_3^-, is considered stored. The Br_2 production rate per area of anode is, therefore, defined as the rate of gain of Br_2 in either form, in the anolyte alone, which is formulated as the product of the average flow rate and the change in average concentration from entrance to exit, per area of anode. Thus

$$P_{Br_2} = [(c_{Br_2,avg,A} + c_{Br_3^-,avg,A})_{x=L} - (c_{Br_2,feed,A} + c_{Br_3^-,feed,A})] \frac{v_{avg}S_AW}{LW} \qquad [31]$$

where $c_{i,avg,A}(x)$ is the local average radial concentration in the anolyte section. Taking into account the laminar flow of the electrolyte, this average concentration is [see Mader *et al.* (12)]

$$c_{i,avg,A}(x) = \frac{6}{S_A} \int_0^{S_A} \left(\frac{y}{S_A} - \frac{y^2}{S_A^2} \right) c_i(x, y)dy \qquad [32]$$

A similar definition may be written for the local radial average concentration in the catholyte section. Storage of Zn is accomplished solely by plating Zn^{2+} ions on the cathode. The production rate of Zn, then, can be found from the rate of the zinc reaction, $i_{n3,avg}$, as

$$P_{Zn} = \frac{(s_{Zn^{2+},3})(i_{n3,avg})}{n_3\mathbf{F}} \qquad [33]$$

A third characteristic which is desirable in a battery, during the charging process, is a low rate of energy consumption relative to the rate of storage of the product. The rate of energy consumption is the product of the applied voltage and the total cell current. The charging rate is equivalent to the rate of production, P_iLW. So, in general, the energy consumption per mole of product stored can be defined as

$$\omega_i = \frac{(E_{cell})(i_{avg}LW)}{P_iLW} \qquad [34]$$

Note that the electrode area cancels out. Substituting Eq. [31] for the production rate of Br_2 into Eq. [34] and rearranging yields

$$\omega_{Br_2} = \frac{(E_{cell})(L/v_{avg})}{S_A} \frac{i_{avg}}{\Delta c_{Br_2}} \qquad [35]$$

where $\Delta c_{Br_2} = (c_{Br_2,avg,A} + c_{Br_3^-,avg,A})_{x=L} - (c_{Br_2,feed,A} + c_{Br_3^-,feed,A})$. The energy consumption per mole of Zn stored is defined by using Eq. [33] for P_{Zn}, giving

$$\omega_{Zn} = \left(\frac{n_3\mathbf{F}}{s_{Zn^{2+},3}} \right) (E_{cell}) \left(\frac{i_{avg}}{i_{n3,avg}} \right) \qquad [36]$$

A final characteristic desirable in a rechargeable battery is a high energy efficiency, a quantity related to the energy consumption term. The energy efficiency is defined as the product of the coulombic efficiency and the voltaic efficiency

$$\epsilon_T = \epsilon_C\epsilon_V \qquad [37]$$

The coulombic efficiency is a measure of the fraction of current passed which gives the desired reaction. At the anode, the Br_2 reaction runs uncontested so that the coulombic efficiency is unity. The coulombic efficiency of more interest is the current efficiency at the cathode, which is defined as

$$\epsilon_C = \frac{|i_{n3,avg}|}{i_{avg}} \quad [38]$$

The voltaic efficiency on charge is defined as the ratio of the theoretical voltage required for charging, to the actual applied voltage. The theoretical required voltage is given by the open-circuit potential of the cell based on the reference conditions. That is, it is the difference of the half-cell potentials for the desired reactions. Therefore, the voltaic efficiency on charge is given by

$$\epsilon_V = \frac{U_{1,ref} - U_{3,ref}}{E_{cell}} \quad [39]$$

The applied cell potential, E_{cell}, includes the two causes of voltaic inefficiency, the overpotentials, η_j, defined earlier in conjunction with the Butler-Volmer equation, and the potential drop across the cell due to ohmic resistance of the separator and the electrolyte. The potential drop across the cell, or IR drop, is defined as

$$\text{IR drop} = \Phi_{0a} - \Phi_{0c} \quad [40]$$

where Φ_{0a} and Φ_{0c} are the potentials of the electrolytic solution at the Br_2 electrode and Zn electrode, respectively.

Substituting the definitions of coulombic and voltaic efficiencies into Eq. [37], the total energy efficiency of the cell on charge may be rewritten as

$$\epsilon_T = \frac{|i_{n3,avg}|(U_{1,ref} - U_{3,ref})}{(i_{avg})(E_{cell})} \quad [41]$$

which is the fraction of energy applied to the cell that leads to useful storage of energy. Note that this definition of total energy efficiency does not take into account energy losses external to the charging process, such as the energy required to pump the electrolyte or the heat losses caused by friction. A procedure for estimating such additional losses is given by Van Zee *et al.* (5).

The energy efficiency as defined in Eq. [41] may be used to redefine the energy consumption per mole of Zn. Solving Eq. [41] for E_{cell}, substituting into Eq. [36] and rearranging gives

$$\omega_{Zn} = \frac{(U_{1,ref} - U_{3,ref})|n_3 F/s_{Zn^{2+},3}|}{\epsilon_T} \quad [42]$$

which indicates that the energy consumption per mole of Zn is a function of only ϵ_T and fixed system parameters. Note particularly that ω_{Zn} is a minimum when the energy efficiency is 100%. Using the values in Table I for the constants in Eq. [42] and assuming 100% efficiency, the minimum possible energy consumption per mole of Zn produced is 344.1 kJ/mol Zn. A similar calculation for Br_2 yields the same value of minimum energy consumption of 344.1 kJ/mol Br_2, since at 100% efficiency 1 mol of Zn is produced for every mole of Br_2 stored.

Table II. Demonstration that the effective separator thickness is an independent parameter

Input parameters: L/v_{avg} = 15s, E_{cell} = 1.9V, $S_A = S_C$ = 0.065 cm

N_m	S_S (cm)	$N_m S_S$ (cm)	$S = S_A + S_S + S_C$ (cm)	ϵ_T	i_{avg} (mA/cm²)
2.0	0.06	0.12	0.19	0.6322	20.54
3.0	0.04	0.12	0.17	0.6322	20.54
6.0	0.02	0.12	0.15	0.6322	20.54

Effective separator thickness.—A simple verification that the product $N_m S_S$ is an independent parameter in a cell with a separator, and not N_m or S_S separately, is given in Table II. While keeping L/v_{avg}, E_{cell}, and S_A constant, the reactor performance is the same when N_m and S_S are adjusted, as long as the effective separator thickness, $N_m S_S$, is held constant. Note that Table II also shows that the total cell gap, S, may be adjusted without affecting the reactor performance, thus verifying that S is not an independent parameter for a separated cell.

Comparison of the one-step and the continuous models.—A comparison of performance criteria for the Zn/Br_2 cell as predicted by the one-step and by the continuous models is presented in Table III. The continuous model for the Zn/Br_2 cell employs a variety of axial step sizes in order to step down the reactor as quickly as possible and still retain accuracy to three digits in solving for c_i and Φ. To achieve this accuracy, step sizes on the order of $\Delta\zeta = 10^{-5}$ are required at the entrance due to the large driving force instantaneously applied, while in the last 60% of the reactor length, step sizes of $\Delta\zeta = 0.01$ are acceptable. The agreement between the one-step and continuous models is as good as 1.3%, for IR drop in the case shown. The worst agreement between the two techniques is for ϵ_T, at 5.6% in the case shown. The agreement is very good for the Zn/Br_2 cell because the fractional conversion of reactant is small, about 1.3% for Br^- and 0.8% for Zn^{2+} when S_A = 0.065 cm. As the channel width, S_A, gets smaller, the conversion increases due to a smaller reactor volume. Accordingly, the agreement between models worsens, to about 10% for ϵ_T when S_A = 0.02 cm, at which the conversion for Br^- is about 4.1% and for Zn^{2+} is about 2.6%. Because the agreement is good and the difference in computation time is so great (up to 100 times faster for the one step), the one-step model is used in all subsequent work to predict the performance of the cell.

Performance predictions at the initial state of charge.—The Zn/Br_2 cell model can be used to predict cell

Table III. Comparison of the one step to the continuous model for the Zn /Br_2 cell

Input parameters: L/v_{avg} = 15s, E_{cell} = 1.9V
S_A = 0.065 cm, $N_m S_S$ = 0.18 cm

		One step	Continuous	% Difference (from continuous)
i_{avg}	(mA/cm²)	19.69	20.02	1.6
IR drop	(mV)	15.146	15.347	1.3
P_{Br_2}	(mol/cm²s) × 10^8	10.307	10.495	1.8
P_{Zn}	(mol/cm²s) × 10^8	6.724	6.471	3.9
ϵ_T		0.619	0.586	5.6
Computation time on CDC CYBER 170/825	(CPU s)	97.0	10,080.	

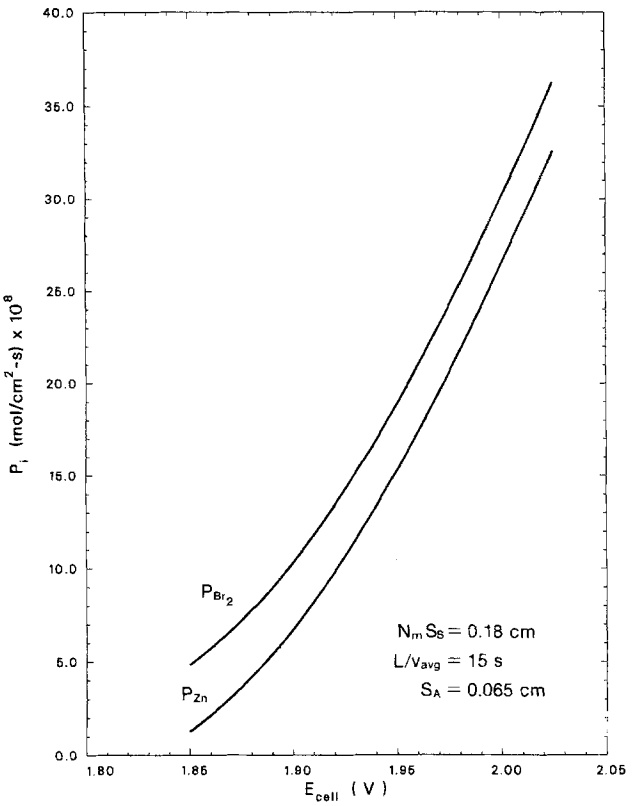

Fig. 2. The effect of applied cell potential on the production rate per area of electrode, of Br_2 and Zn, at initial charging conditions.

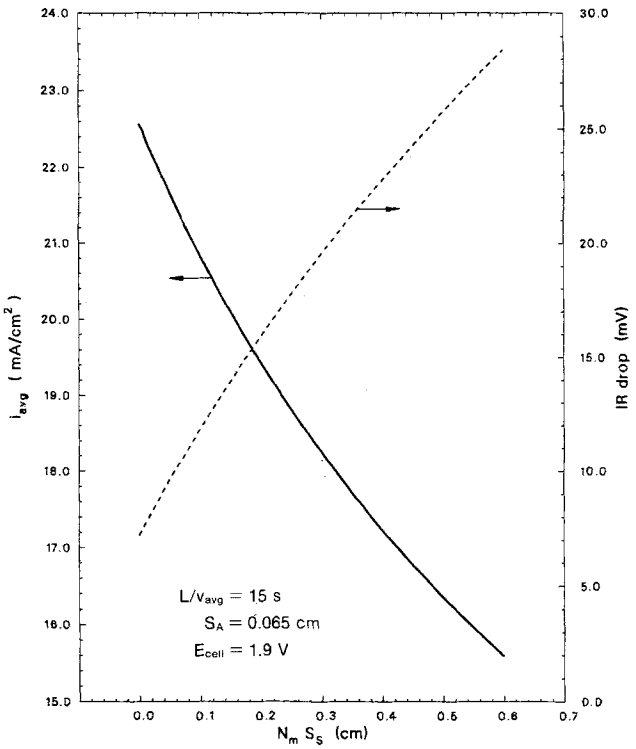

Fig. 4. The effect of effective separator thickness on the average current density and potential drop across the cell, at initial charging conditions.

performance at a specific state of charge as a function of any of the independent parameters. Figures 2-5 show some of the performance predictions that can be made at the initial state of charge corresponding to the feed concentrations listed in Table I.

For instance, the predicted effect of E_{cell} on P_{Br_2} and P_{Zn}, at initial charging conditions, is shown in Fig. 2. Note that the rate at which Br_2 is stored is significantly different from the rate at which Zn is stored. It is important that P_{Br_2} is not greater than P_{Zn} throughout all states of charge, since the amount of product (Br_2 and Zn) and of reactant (Br^- and Zn^{2+}) would become greatly mismatched quickly, causing battery failure. This problem is resolved when considering performance under charging conditions. Figure 2 also suggests that the battery can be

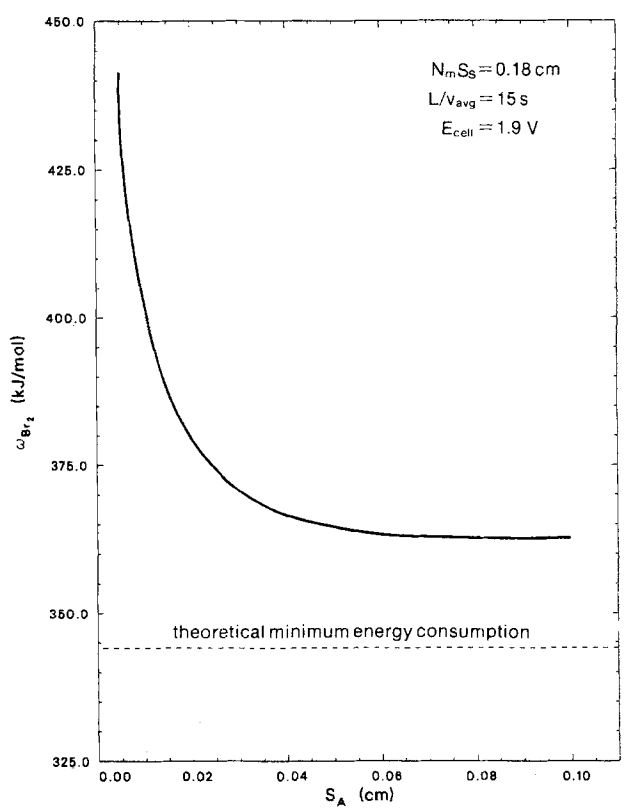

Fig. 3. The effect of channel width on the energy consumption per mole of Br_2 stored, at initial charging conditions.

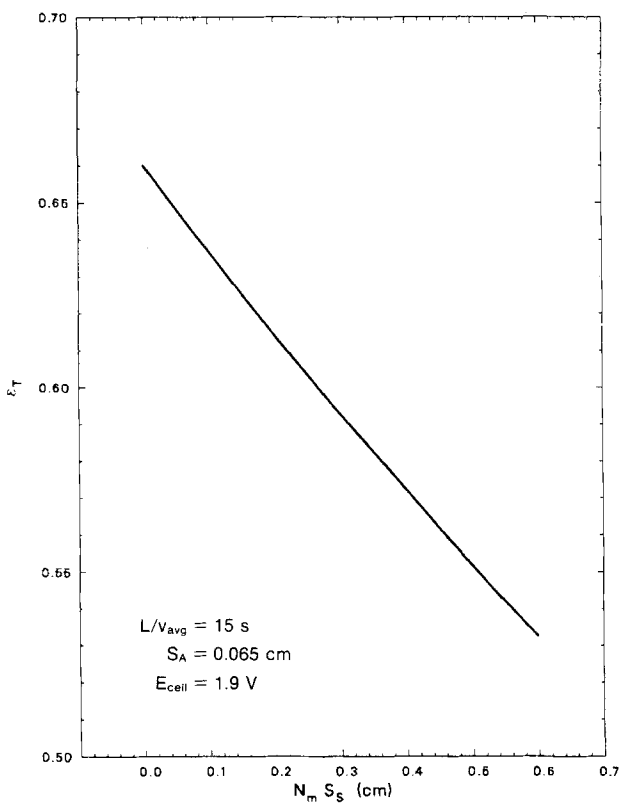

Fig. 5. The effect of effective separator thickness on the total energy efficiency, at initial charging conditions (ϵ_V = 0.9384).

charged about as rapidly as desired, by increasing the applied cell potential. However, since the amount of current passed will also increase with E_{cell}, the maximum allowable value of current density to avoid dendrite growth must be carefully considered.

In Fig. 3, the predicted effect of S_A on the energy consumption per mole of Br_2, ω_{Br_2}, is illustrated at initial charging conditions. The dashed line indicates the theoretical minimum value of ω_{Br_2}, 344.1 kJ/mol of Br_2. At values of S_A less than 0.02 cm, the energy consumption per mole of Br_2 stored rises unacceptably high, while for values of S_A greater than 0.05 cm, ω_{Br_2} levels out to about 363. kJ/mol of Br_2. Figure 3 shows that, at the initial state of charge, the energy consumption per mole of Br_2 is dramatically and adversely affected by narrow flow channels. It suggests that designing a cell with channel widths of less than 0.02 cm is not advisable.

Figure 4 illustrates the predicted effect of N_mS_S on the IR drop and on i_{avg}, at initial charging conditions. Figure 4 shows that the potential drop increases as N_mS_S increases, as expected, since the separator contributes to the overall cell ohmic resistance. Figure 4 also shows that the average current density drops with increasing N_mS_S since the cell mass-transfer resistance is increased by the thicker separator.

Figure 5 demonstrates the predicted effect of N_mS_S on the total energy efficiency at initial charging conditions. Because E_{cell} is fixed at 1.9V, the voltaic efficiency is fixed at $\epsilon_V = 1.783/1.9 = 0.9384$. Thus, Fig. 5 is actually a measure of the change of coulombic efficiency with effective separator thickness. At initial charging conditions, the relationship between ϵ_T and N_mS_S is nearly linear, with the efficiency surprisingly dropping as the separator resistance increases. This performance suggests that, at least at the state of charge considered, the increased mass transfer and ohmic resistance of the separator unfortunately influences the cell performance more strongly than does the beneficial aspect of preventing Br_2 diffusion from the anode to the cathode. This trend is reversed as charging continues, as discussed below.

Performance predictions at various states of charge.—Figures 6-11, in which the state of charge is followed for three values of N_mS_S (Fig. 6-8) and three values of L/v_{avg} (Fig. 9-11), resolve the problems found of mismatched production rates and poorer performance as the effective separator thickness is increased at the initial state of charge.

Although pseudo-steady state is assumed in the model, the concentration and potential distributions in the cell do change over long periods of time, and therefore the state of charge and cell performance also change. Bellows of Exxon (13) has determined that a convenient parameter for following the state of charge of a Zn/Br_2 battery is the amount of Zn^{2+} which has been consumed and deposited as Zn. The percentage of Zn^{2+} plated as solid Zn,

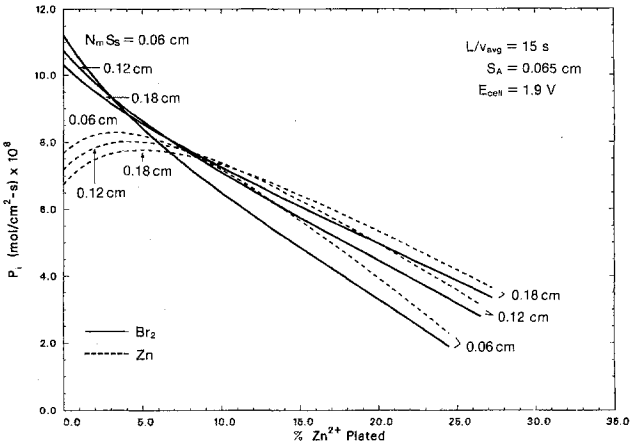

Fig. 7. The effect of effective separator thickness on production rate per area of electrode, under charging conditions.

then, can be defined as the difference between the original amount of Zn^{2+} introduced as feed to the system and the amount of Zn^{2+} currently entering the cell. The initial feed concentration of Zn^{2+} introduced to both channels of the cell is $c_{Zn^{2+},ref}$, while the amount currently entering the system is $c_{Zn^{2+},feed,A}$ in the anolyte and $c_{Zn^{2+},feed,C}$ in the catholyte. Therefore, the percentage of Zn^{2+} plated relative to the start-up concentration of Zn^{2+} is

$$\%Zn^{2+}\text{ plated} = 100\% \times \left[\frac{S_A(c_{Zn^{2+},ref} - c_{Zn^{2+},feed,A}) + S_C(c_{Zn^{2+},ref} - c_{Zn^{2+},feed,C})}{S_A(c_{Zn^{2+},ref}) + S_C(c_{Zn^{2+},ref})}\right] \quad [43]$$

or, when $S_A = S_C$,

$$\%Zn^{2+}\text{ plated} = 100\% \times [1.0 - 0.5(\theta_{Zn^{2+},feed,A} + \theta_{Zn^{2+},feed,C})] \quad [44]$$

Bellows (13) claims that when approximately 70% of the Zn^{2+} ions are plated, the system is fully charged. Because of the large amount of computer time required to follow the state of charge, studies were limited to approximately 25% of Zn^{2+} plated.

In order to follow the concentration distribution as a function of the state of charge, it is necessary to assume that the exit average concentration of each species in each channel, at a known state of charge, will be the feed concentration of each species for that particular channel at some later state of charge. That is, it is reasonable to assume that since the composition of anolyte and catholyte is assumed to change slowly under pseudo-steady-state conditions, then the composition leaving the cell at any state of charge will eventually be duplicated in the storage tanks and thus in the feed to the anolyte and catholyte channels. Also, it is assumed that the anolyte is

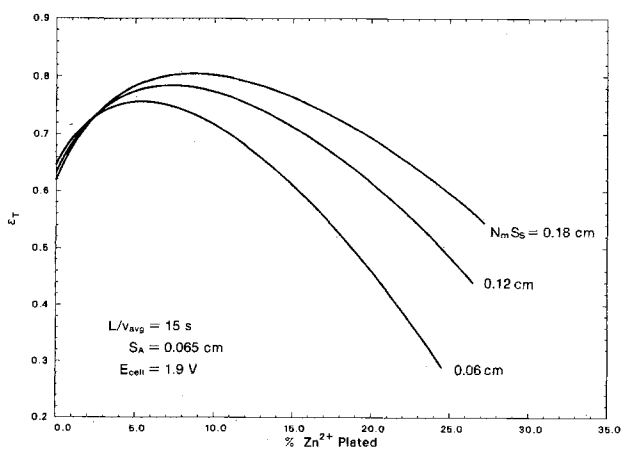

Fig. 6. The effect of effective separator thickness on energy efficiency, under charging conditions (ϵ_V = 0.9384).

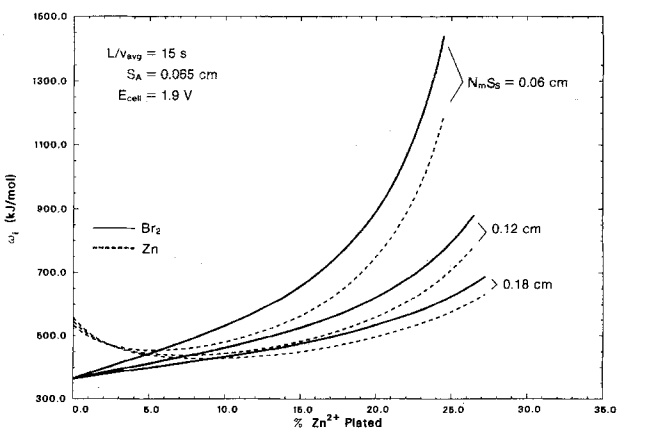

Fig. 8. The effect of effective separator thickness on energy consumption, under charging conditions.

stored in a tank separate from the catholyte tank, so that the feed composition of each channel changes independently. Although the assumptions that the process is under pseudo-steady-state conditions and that the exit composition at one state of charge is the feed composition at a future state of charge are valid only for very low conversion, these assumptions at least present a rough estimate of the performance possible as a function of the state of charge.

Cases studied under charging conditions include three effective thicknesses of the separator and three settings of residence time, under otherwise fixed conditions. For all cases, the start-up composition of the electrolyte is the same as that used to study initial charging conditions. The applied cell potential and channel are also fixed, with E_{cell} = 1.9V and S_A = 0.065 cm. For the cases in which the effective separator thickness is varied, L/v_{avg} is fixed at 15s and the three values of N_mS_S studied are 0.06, 0.12, and 0.18 cm. For the cases in which the residence time is varied, N_mS_S = 0.18 cm and the three values of L/v_{avg} studied are 10, 15, and 20s. These cases were chosen as representative of typical cell designs. The performance of the cells with different separators under charging conditions is shown in Fig. 6-8 and the performance of the cells at different residence times is shown in Fig. 9-11.

The predicted effect of N_mS_S on ϵ_T under charging conditions is demonstrated in Fig. 6. For each of the three cases shown, ϵ_T improves through the initial charging process, levels off at a maximum efficiency, and then drops steadily as the cell is charged further. At initial charging conditions, up to about 2% of Zn^{2+} storage, the efficiency is best for the cell with the thinnest separator (0.06 cm) and worst for the cell using the thickest separator (0.18 cm). This behavior is due to the differences in cell mass transfer and ohmic resistance for the three separators. As the charging process continues, however, ϵ_T becomes optimum for the cell with the thickest separator and the lowest for the cell with the thinnest separator considered, as shown in Fig. 6. In addition, the discrepancy between cell designs becomes more pronounced as the amount of charge progresses. Figure 6 shows, therefore, that the separator overcomes the disadvantage of an increased cell resistance when the effective thickness of the separator is increased, by minimizing the amount of Br_2 which diffuses from the anolyte to the catholyte. Therefore, a thicker separator is necessary to improve the cell energy efficiency, especially when the cell is to be driven to a high state of charge. For instance, if it is desired to keep ϵ_T above 0.5 through a state of charge of 30% Zn^{2+} plated, then N_mS_S must be greater than 0.18 cm.

The response of P_{Br_2} and P_{Zn} to the three cells of various effective separator thickness, as charging progresses, is shown in Fig. 7. Again, for the lowest states of charge, the cell with the separator of width 0.06 cm shows the best performance, having the highest production rate for either Br_2 or Zn, but as charging continues, the production rate drops to the lowest of the three cases considered.

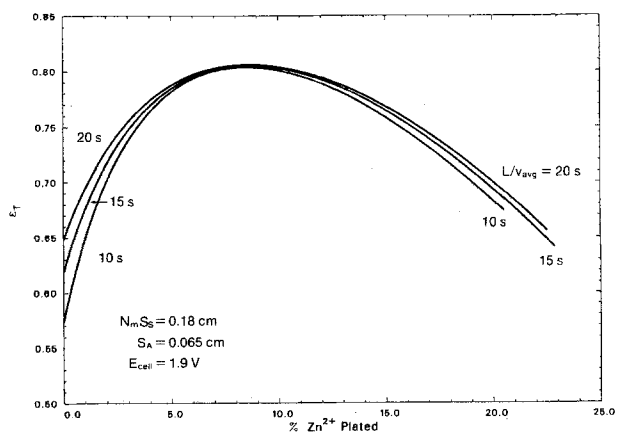

Fig. 9. The effect of residence time on energy efficiency, under charging conditions (ϵ_V = 0.9384).

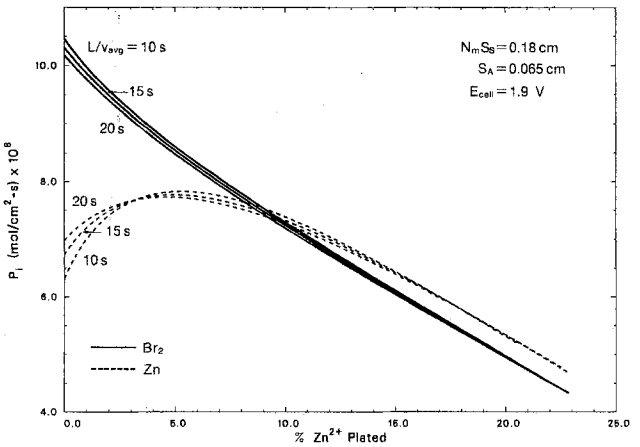

Fig. 10. The effect of residence time on production rate per area of electrode, under charging conditions.

Likewise, the thickest separator, at 0.18 cm, has the slowest production rate at initial charging conditions, but shows the best performance at the highest states of charge.

At initial charging conditions, P_{Zn} is significantly less than P_{Br_2}, but as the state of charge increases to the moderate to high range, Zn is deposited faster than Br_2 is stored, for each of the cells considered. This behavior is important to the success of the Zn/Br_2 battery. Because the battery is a closed system, it is necessary that in a complete cycle of charge and discharge, Br_2 is not produced in excess of the amount of Zn deposited, and vice versa. Figure 7 shows that although Br_2 is initially produced faster than Zn, fortunately the relative rates reverse so that through a full charging process, the amounts of each stored species will be approximately equivalent. Integration of P_{Br_2} and P_{Zn} over the length of charge will indicate whether Br_2 or Zn^{2+} is lost in each cycle, allowing prediction of the number of cycles until the concentrations are badly mismatched.

In Fig. 8, the energy consumption based on both Br_2 and Zn is illustrated as charging progresses, for the three values of N_mS_S. As the cell is charged, ω_{Br_2} increases quite dramatically and is particularly sensitive to the thickness of the separator. At an initial state of charge, the value of ω_{Br_2} is identical for every value of N_mS_S, but as the state of charge progresses past 20% of the Zn^{2+} ions deposited, the energy required to produce and store a mole of Br_2 when N_mS_S is 0.06 cm is more than double that required when N_mS_S is 0.18 cm. The value of ω_{Zn} is likewise sensitive to the effective thickness of the separator.

As with the production rates, it is important that the energy consumed to produce and store each of Br_2 and Zn be equivalent for a full cycle of the battery. Figure 8 demonstrates that over a large amount of charging, the energy consumption per mole of Zn is about the same as the consumption per mole of Br_2.

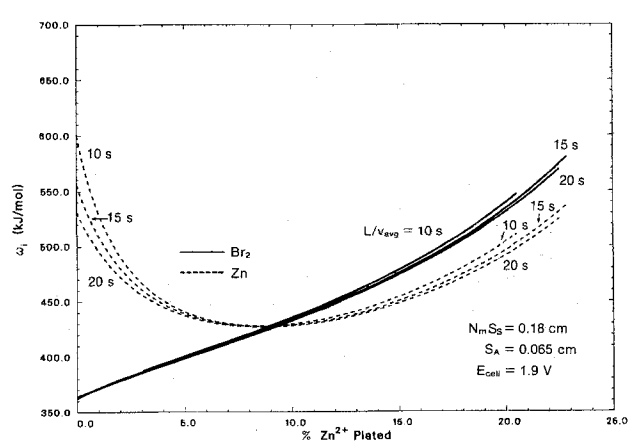

Fig. 11. The effect of residence time on energy consumption, under charging conditions.

Consideration of Fig. 6-8 as a whole shows that of the three separators considered, the thickest one, with $N_m S_S$ = 0.18 cm, is by far the best. This thickness gives the highest efficiency and production rates of Br_2 and Zn per area of electrode, over the range of charge considered, and provides a dramatically lower energy consumption per mole of both Br_2 and Zn. In addition, when $N_m S_S$ has a value of 0.18 cm. Fig. 6-8 suggest that to achieve the best battery, charging should be begun approximately when the status of the battery is at a state of charge of 5% Zn^{2+} plated, rather than at a fully discharged state, and that the battery should be charged up only to a 20% deposit of Zn^{2+} ions. Within this range of charge, ϵ_T, P_{Zn}, and ω_{Zn} all reach optimum values and P_{Br_2} and ω_{Br_2} deteriorate, but at acceptable rates. On the other hand, at states of charge lower than 5% Zn^{2+} plated, ϵ_t, P_{Zn}, and ω_{Zn} exist at decidedly nondesirable values, while at states of charge higher than a 20% deposit of Zn^{2+} ions, performance criteria begin to deviate from their optimum values rapidly.

In Fig. 9-11, a change in residence time on cell performance under charging conditions is shown to have little effect. Figure 9 shows that varying the residence time between values of 10, 15, and 20s has only a slight effect on ϵ_T, and the divergence that occurs is most pronounced at initial charging states or when the battery is charged for extended periods of time.

In Fig. 10, again there is very little variance in production rates of either Br_2 or Zn as the residence time is changed. Perhaps most remarkable is that at the highest states of charge illustrated (above 15% deposition of Zn^{2+}), the production rate of Br_2 per surface area of anode is equivalent for all three residence times. Note that P_{Zn}, starts out at an initial state of charge very low relative to the rate of storage of Br_2. P_{Zn} rises slightly and then drops off slower than P_{Br_2}, with Zn eventually being produced at a rate higher than Br_2 is stored. Such behavior again is desired, because over a cycle of charge and discharge, it is important that neither excess Br_2 nor excess Zn be produced.

In Fig. 11, through all states of charge, ω_{Br_2} diverges very little due to different values of L/v_{avg}. On the other hand, ω_{Zn} is shown to be unaffected by L/v_{avg} only when the energy consumption is at its most optimum, between a 5% and 10% deposition of Zn^{2+}. A residence time of 20s provides the minimum value of ω_{Zn} for all states of charge.

Consideration of Fig. 9-11 shows that a change of residence time has little effect on overall cell performance, whether efficiency, production rate, or energy consumption. This is especially true relative to the change in performance undergone, as charging progresses, when $N_m S_S$ is varied. The optimum value of L/v_{avg}, among the three values considered, is the largest time, 20s. The trends shown suggest that lengthening the residence time beyond 20s will further enhance the predicted performance. If the charging process is restricted between 5 and 20% of Zn^{2+} plated as discussed earlier, however, then Fig. 9-11 indicate that the value of L/v_{avg} used has virtually no effect on ϵ_T, P_i, or ω_i.

Conclusions

The Zn/Br_2 cell model presented is a useful tool to aid in the design of a complete battery system. Its ability to predict accurately the performance of cells within batteries currently under development by Exxon, ERC, and others is untested because data are very limited for proprietary reasons. However, it is a versatile model which can be extended easily or modified to fit assumptions not used here. In addition, the model can be used in conjunction with a parameter estimation technique and experimental results from a working cell to determine unknown system constants such as diffusivities, D_i, exchange current densities, $i_{oj,ref}$, and reaction transfer coefficients, α_{aj}, and α_{cj}.

Acknowledgment

This work was supported in part by the Center for Energy and Minerals Research at Texas A&M University.

Manuscript received July 19, 1985.

LIST OF SYMBOLS

c_i	concentration of species i, mol/cm^3
$c_{i,avg,A}$	average concentration of species i in the anolyte channel, mol/cm^3
$c_{i,feed}$	feed concentration of species i, mol/cm^3
$c_{i,ref}$	reference concentration of species i, mol/cm^3
D_i	diffusion coefficient of species i, cm^2/s
$D_{i,e}$	effective diffusion coefficient of species i in the separator, cm^2/s
d_o	density of pure solvent, kg/cm^3
D_R	diffusion coefficient of limiting reactant, cm^2/s
E_{cell}	applied cell potential (= $V_a - V_c$), V
$\mathbf{F}$	Faraday's constant, 96,487 C/mol
I	total cell current, mA
i_{avg}	average current density at an electrode (= I/LW), mA/cm^2
i_{nj}	normal component of current density due to reaction j, mA/cm^2
$i_{nj,avg}$	average normal current density due to reaction j, mA/cm^2
$i_{oj,ref}$	exchange current density of reaction j, mA/cm^2
IR drop	potential drop across the cell (= $\Phi_{oa} - \Phi_{oc}$), V
K_{eq}	equilibrium constant for tri-bromide reaction, cm^3/mol
L	electrode length, cm
L/v_{avg}	residence time of the reactor, s
$\mathbf{N}_i$	flux vector of species i, mol/cm^2-s
n_j	number of electrons passed in reaction j
N_m	MacMullin number in the separator
$N_m S_S$	effective separator thickness, cm
N_{ni}	normal component of the flux (y- or η-direction) of species i, mol/cm^2-s
P_i	production rate of species i per electrode area,mol/cm^2-s
p_{ij}	anodic reaction order of species i in reaction j
Pe	Peclet number (= $2Sv_{avg}/D_R$)
q_{ij}	cathodic reaction order of species i in reaction j
R	gas law constant, 8.314 J/mol-K
R_i	homogeneous reaction rate, mol/cm^3-s
S	total electrode gap, cm
S_A	anolyte channel width, cm
S_C	catholyte channel width, cm
s_{ij}	stoichiometric coefficient of species i in reaction j
S_S	width of the separator, cm
T	temperature, K
U_j^θ	standard half-cell potential, V
$U_{j,ref}$	open-circuit potential of reaction j based on the reference concentrations, V
$\mathbf{v}$	electrolyte velocity vector, cm/s
V_a	anode potential, V
v_{avg}	average velocity of the electrolyte, cm/s
V_c	cathode potential, V
V_e	potential of electrode, V
v_x	velocity component of the electrolyte in the x-direction, cm/s
W	breadth of the electrode, cm
x	axial coordinate, cm
y	normal coordinate, cm
z_i	charge number of species i

Greek

α	aspect ratio, S/L
α_{aj}	anodic transfer coefficient for reaction j
α_{cj}	cathodic transfer coefficient for reaction j
Δc_{Br_2}	difference in average concentration of bromine-carrying species (Br_2 and Br_3^-) from entrance to exit, mol/cm^3
ϵ_C	coulombic efficiency
ϵ_T	total cell energy efficiency
ϵ_V	voltaic efficiency
ζ	dimensionless axial coordinate (x/L)
η	dimensionless normal coordinate (y/S)
η_j	overpotential at electrode surface ($V_e - \Phi_{oe} - U_{j,ref}$), V
η'	dimensionless normal coordinate, specific to a flow channel
θ_i	dimensionless concentration of species i ($c_i/c_{i,ref}$)
$\theta_{i,feed}$	dimensionless feed concentration of species i
$\theta_{i,o}$	dimensionless concentration of species i at the electrode surface
ρ	resistivity of separator and its surrounding electrolytic solution, Ω-cm
ρ_o	resistivity of the pure electrolytic solution, Ω-cm

Φ solution potential, V
Φ_{oa} solution potential at the anode, V
Φ_{oc} solution potential at the cathode, V
Φ_{oe} solution potential at electrode, V
ω_i energy consumption per mole of product stored, kJ/mol

REFERENCES

1. J. L. Chamberlin, in "Proceedings of the EPRI/LBL Workshop on the Electrochemistry of Zinc/Halogen Batteries," Palo Alto, CA, Nov. 30-Dec. 1, 1983, Vol. I, p. 2-15 (1984).
2. R. E. White, M. Bain, and M. Raible, *This Journal*, **130,** 1037 (1983).
3. J. Lee and J. R. Selman, *ibid.*, **129,** 1670 (1982).
4. J. Lee, Ph. D. Dissertation, Illinois Institute of Technology, Chicago, IL (1981).
5. J. Van Zee, R. E. White, P. Grimes, and R. Bellows, in "Electrochemical Cell Design," R. E. White, Editor, p. 293, Plenum Press, New York (1984).
6. P. S. Fedkiw and R. W. Watts, *This Journal*, **131,** 701 (1984).
7. J. Van Zee, Ph.D. Dissertation, Texas A&M University, College Station, TX (1984).
8. T. Nguyen, C. Walton, R. E. White, and J. Van Zee, *This Journal*, Submitted for publication.
9. M. Eigen and K. Kustin, *J. Am. Chem. Soc.*, **84,** 1355 (1962).
10. D. J. Pickett, "Electrochemical Reactor Design," 2nd ed., Elsevier Scientific Publishing Co., New York (1979).
11. R. E. White, S. E. Lorimer, and R. Darby, *This Journal*, **130,** 1123 (1983).
12. M. Mader, C. Walton, and R. E. White, *ibid.*, **133,** 1124 (1986).
13. R. Bellows, in "Proceedings of the EPRI/LBL Workshop on the Electrochemistry of Zinc/Halogen Batteries," Palo Alto, CA, Nov. 30-Dec. 1, 1983, Vol. I, p. 4-3 (1984).
14. R. Bellows, P. Grimes, H. Einstein, E. Kantner, P. Malachesky, and K. Newby, *IEEE Trans. Veh. Technol.*, **vt-32,** 26 (1983).
15. "CRC Handbook of Chemistry and Physics," 60th ed., CRC Press, Inc., Boca Raton, FL (1979).
16. J. S. Newman, "Electrochemical Systems," Prentice Hall, Inc., Englewood Cliffs, NJ (1973).
17. R. E. White, in "Proceedings of the EPRI/LBL Workshop on the Electrochemistry of Zinc/Halogen Batteries," Palo Alto, CA, Nov. 30-Dec. 1, 1983, Vol. I, p. 5-65 (1984).
18. R. Selman, in "Proceedings of the EPRI/LBL Workshop on the Electrochemistry of Zinc/Halogen Batteries," Palo Alto, CA, Nov. 30-Dec. 1, 1983, Vol. II, p. 10-63 (1984).
19. P. Grimes, in "Proceedings of the EPRI/LBL Workshop on the Electrochemistry of Zinc/Halogen Batteries," Palo Alto, CA, Nov. 30-Dec. 1, 1983, Vol. II, p. 7-25 (1984).
20. U. Landau, in "Proceedings of the EPRI/LBL Workshop on the Electrochemistry of Zinc/Halogen Batteries," Palo Alto, CA, Nov. 30-Dec. 1, 1983, Vol. II, p. 10-75 (1984).
21. M. Mader, M. S. Thesis, Texas A&M University, College Station, TX (1985).

The Lithium Surface Film in the Li/SO_2 Cell

K. M. Abraham* and S. M. Chaudhri

EIC Laboratories, Incorporated, Norwood, Massachusetts 02062

ABSTRACT

Evidence is presented which suggests that the Li surface film in the Li/SO_2 cell comprises a complex mixture of products which include Li_2S and several Li sulfur-oxy compounds. Elemental analysis, IR spectral, and XPS data indicate that the Li sulfur-oxy compounds may be $Li_2S_2O_4$, Li_2SO_3, $Li_2S_nO_6$, and $Li_2S_2O_5$.

Lithium batteries, particularly those containing liquid electrolytes, owe their stability to protective films on the Li anode surface. These films, formed by spontaneous reaction of Li with the electrolyte solution, have been identified to affect such battery properties as voltage delay (1), anodic polarization (2), self-discharge rates (3), rechargeability (4), and safety (1, 5).

One of the most extensively studied interphases between the Li anode and a liquid electrolyte is the LiCl film in the Li/$SOCl_2$ cell (1, 3). Studies of the morphological and electrical properties of this film have led to the recognition of it as a solid electrolyte interphase (SEI). Such an interphase, while allowing the migration of Li^+ across it, behaves as an electronic insulator preventing self-discharge and serves as a barrier to further reactions between the Li anode and the electrolyte. It is now accepted that a SEI or a conceptually similar film exists in all liquid electrolyte Li batteries and the film is formed instantaneously upon contact of the Li anode with the electrolyte. This compact SEI is believed to be the "protective" film. The latter is often covered by a coarse porous film whose thickness is determined by, among other factors, the length of exposure of the Li electrode to the electrolyte. The chemical composition and physical properties of Li surface films have also been studied in PC/$LiClO_4$ (6), THF/$LiAsF_6$ (7), and Li_2S_n (8).

It has been believed all along that the Li surface film in the Li/SO_2 cell solely comprised $Li_2S_2O_4$ (1). However, recent studies have begun to indicate a more complex composition for the film. Auger spectroscopic results of Nebesny *et al.* (9) of fresh Li surfaces after exposure to low levels of SO_2 indicated the presence of Li_2S and Li_2O. X-ray photoelectron spectroscopic (XPS) studies of similar Li surfaces by Hoenigman and Keil (10) showed the presence of Li sulfur-oxy compounds in addition to Li_2O and Li_2S. The latter authors also found only Li_2O and Li_2S at low levels of SO_2 exposure. With longer SO_2 exposure, however, they observed the evolution of XPS peaks at 168.8, 166, and probably 163.2 eV. Considering that only 1.3 eV separates the 163.2 eV peak from the Li_2S main peak at 161.9 eV, the former could be the 2Pl/2 transition of the sulfide. The sulfur 2Pl/2 · 3/2 doublet separation, evaluated from the spectra of a number of Li sulfur-oxy compounds, is ~1 eV. The peak at 168.8 eV was assigned to Li_2SO_3. No assignment was given to the peak at 166 eV. Recently we reported (11) on the composition of the Li surface film found on the anodes of partially discharged and stored Li/SO_2 cells. Infrared (IR) spectral and XPS analyses of the film indicated the presence of several Li sulfur-oxy compounds including $Li_2S_2O_4$ and $Li_2S_nO_6$. Lately, we have examined by SEM, IR, and XPS, the Li surfaces of a large number of Li/SO_2 cells after they have been subjected to various regimes of discharge, such as partial and full discharge at low to moderate rates, high current pulse discharge, and forced overdischarge. The results of these studies have led us to conclude that the Li surface film in the Li/SO_2 cell comprises a complex mixture of products including several Li sulfur-oxy compounds and Li_2S. Our results are reported in this paper.

Experimental

All the experiments involving manipulation of air sensitive materials were carried out inside a Vacuum Atmo-

* Electrochemical Society Active Member.